Proceedings of GT2009
ASME Turbo Expo 2009: Power for Land, Sea and Air
June 8-12, 2009, Orlando, Florida, USA

GT2009-59590

Overspray Fog Cooling in Compressor using Stage-Stacking Scheme with Non-Equilibrium Heat Transfer Model for Droplet Evaporation

Jobaidur R. Khan and Ting Wang
Energy Conversion & Conservation Center
University of New Orleans
New Orleans, LA 70148-2220, USA

ABSTRACT

The inlet fog cooling scheme has been proven as an economic and effective means to augment gas turbine output power on hot or dry days. A previous paper developed a stage-by-stage wet-compression theory for overspray and interstage fogging using the equilibrium droplet evaporation model with given compressor and blade configurations. This paper extends the previous work by including the non-equilibrium droplet heat transfer model.

An 8-stage, 2-D compressor airfoil geometry and stage settings at the mean radii are employed. Eight different cases including saturated fogging, overspray with different droplet sizes with both equilibrium and non-equilibrium heat transfer models have been investigated and compared. The results show saturated fogging increases the pressure ratio and reduces the compressor power consumption; however, overspray actually increases both the specific and total compressor power consumption. Non-equilibrium method differs from the equilibrium method due to the change of evaporation rate. Droplet size doesn't play a role in equilibrium approach, but plays a major role in affecting the result in the non-equilibrium case. For small droplet size of 10 μm, the droplet evaporation rate is fast, so the non-equilibrium method predicts close results as the equilibrium method. Larger droplets lead to slower evaporation, reduction of pressure ratio, and less effective compressor performance than the smaller droplets. Equilibrium method predicts that wet compression increases axial velocity, blade inlet velocity, incidence angle, and tangential component of velocity. Non-equilibrium methods predict a similar trend except with lesser increments as the droplet size increases. In the present study, the equilibrium method predicts that all the water droplets evaporate completely at the end of stage 3, while the non-equilibrium approach predicts that the completion of evaporation delays, but all droplets completely evaporate in the compressor except the biggest droplets (30μm). Saturated fogging increases air density; however, both equilibrium and non-equilibrium methods predict that overspray wet compression actually reduces air density in the earlier 70% of the compressor. Non-equilibrium predicts small droplets relax the load in the earlier stages but increases the load in the later stages. Larger droplets show less load changes. Detailed stage-to-stage performance and property value changes are analyzed and discussed in this study.

NOMENCLATURE

A	Surface Area
d	Droplet Diameter (μm)
D	Mass Coefficient of Diffusion (m^2/s)
D.A.	Dry Air
Cp	Specific Heat (kJ/kg.K)
GT	Gas Turbine
h	Heat Transfer Coefficient ($W/m^2.K$)
h_{fg}	Latent Heat of Evaporation (kJ/kg)
k	Thermal Conductivity (W/m.K)
L	Blade Chord Length
m	Mass (kg)
Nu	Nusselt Number (≡hd/k)
P	Pressure (kPa)
Pr	Prandtl Number (≡μCp/k)
P_r	Pressure ratio
R	Gas Constant for Air (0.287 kJ/kg-K)
Re	Reynolds Number ($\equiv \rho V_s d/\mu$)
RH	Relative Humidity (%)
t	Time (s)
T	Temperature (K)
U	Tangential Velocity (m/s)
V	Volume (m^3)
V_a	Axial Velocity (m/s)
V_s	Slip Velocity between Droplet and Air (m/s)
W_c	Compressor power
Greek	
ϕ	Flow Coefficient ($\equiv V_a/U$)
μ	Dynamic Viscosity (Pa.s)
ρ	Density (kg/m^3)
τ_e	Evaporation Time (s)
τ_b	Boiling Time (s)
ω_1	Absolute humidity at WBT (kg/kg D.A.)

Superscripts

i	Rotor Stage
i+0.5	Stator Stage

Subscripts

a	Dry Air
d	Droplet
f	Liquid Water Component
g	Water Vapor Component

INTRODUCTION

Compressor intercooling has been proven to be the most economic way to reduce compressor work and augment gas turbine output power, especially during hot or dry days. Conventional intercooling schemes are usually applied through non-mixed heat exchangers between two compressor stages or by cooling the outside of the compressor casing. Another method to cool the compressor is to employ gas turbine inlet cooling by refrigeration or evaporative cooling schemes.

Inlet fogging is one of the evaporative cooling schemes and has been considered a simple and cost-effective method to significantly increase power output and often also increase thermal efficiency. During fog cooling, water is atomized to micro-scaled droplets and introduced into the inlet airflow. The water droplet remaining after the air flow reaching the wet bulb temperature is considered as the overspray (or high fogging), which can further cool the compressor. Recently, interstage fogging is considered to take advantage of the existing on-line compressor washing system. However, any cooling schemes that may affect the flow field inside the compressors have not been favorably considered by industry due to concerns of any disturbance that might damage compressor airfoils or adversely affect the compressor's performance stability. There are several concerns associated with overspray and interstage spray cooling like: (a) the potential erosion of compressor blades caused by tiny water droplets, (b) drilling holes through the compressor casings to install fogging devices may cause a compressor integrity problem, and (c) the manufacturer's warranty could be voided [1]. Regarding interstage fogging, Bagnoli et. al. [2] and Wang and Khan [3, 4] have shown that less power augmentation can be obtained by applying fogging inside the compressor between two stages than upstream of the compressor inlet.

Thermodynamic wet compression theory was established first by Hill [5] in 1963. Since then, incremental developments have led to recently work by Zheng et al. [6, 7]. Their analysis provided the relationship between the dry compression index and wet compression index. Following their work, Khan and Wang [8] developed a wet compression thermodynamic model for a gas turbine system (FogGT) with inlet fog cooling specifically for burning low calorific value (LCV) fuels. The results showed that in the combustor, as heating value decreases for LCV fuels, fogging results in more incombustible gases to absorb the energy and suppress the combustion temperature; so more heat addition (23% - 46%) is required to allow the combusted gas to reach the desired turbine inlet temperature (TIT). When LCV fuels are burned, saturated fogging can achieve a net output power increases approximately 1-2%, while 2% overspray can achieve 20% net output enhancement. Fog/overspray could either slightly increase or decrease the thermal efficiency of LCV-fired GT systems depending on the ambient conditions.

Williams [9] reported the effects of water ingestion (due to heavy rain) on the performance of a low speed four stage laboratory axial flow compressor. He showed how the surge line was adversely affected by water ingestion when the stall initiating stage was adversely affected. For a compressor operating at part speed, it was generally the first stage that initiated stall, and the experimental result was consistent with this. Generally the first stage performance was scarcely different from under dry conditions with water injection. With up to 20% (wt.) water spray, at the stall point, the overall total-to-static pressure rise was reduced, but the stall point remained on the throttle line passing through the stall point of the dry characteristic. This implies no movement of the surge line and results from the near-casing region of the first stage remained relatively dry, due to the high axial momentum of the water taking it through the rotor blade row without being centrifuged to the casing. In contrast, tests with atomizing nozzles produced low axial momentum fine droplets over the entire inlet area and tests with spraying water directly onto the compressor casing ahead of the inlet showed significant adverse effects on both stage one (and later stage) performance and the compressor surge line. He predicted the high-pressure compressor to stall with 2.5% water injection.

Payne and White [10] presented the calculation procedure for evaporative flow of three-dimensional blade rows. They analyzed the injection of small droplets, which were assumed to follow the main flow. Their results showed that the main change in the flow occurred due to the progressive reduction of axial velocity and evaporation. As a result, the blade pressure distribution changed. They acknowledged that further work was required to include all the effects of slip velocity relevant to larger droplets. Abdelwahab [11] applied the wet compression to a centrifugal compressor. He found that small droplet radii led to a much faster evaporation time compared to the fluid particle travel time. The higher the injection rate, the higher the total pressure ratio the stage could develop. This was due to colder compression temperatures allowing the work transferred from the impeller to the flow and then converted into higher total pressures. Sanaye et. al. [12] studied the effects of inlet fogging and wet compression on gas turbine performance. They modeled the evaporation of water droplets in the compressor inlet duct and estimated the diameter of water droplets at end of the inlet duct. They compared their findings with the results from FLUENT software. They also predicted the compressor discharge air temperature with the presence of unevaporated water at the inlet duct. They found that flow coefficient increased in first few stages due to the water spray. This led to the increase in axial velocity at the first few stages and the corrected speed increased due to the cooling of compressor inlet air. The result showed an increase in density and pressure and a decrease in the axial velocity at later compressor stages. The amount of water injection increased with increased pressure ratio.

Bianchi et. al. [13] studied the influence of water droplet size and temperature of wet compression in a 17-stage compressor. They concluded that the gas turbine performance improved for finer and hotter droplets, as the evaporation rate increases with hotter droplets, but their analysis did not consider the cost of preheating water to produce hotter droplets, i.e. treating the preheat energy as free. They also found that the redistribution of compressor stages load with an unloading of the first compressor stages and an overloading of the last compressor stages was influenced by the diameter and temperature of liquid water droplets.

Sexton et. al. [14] conducted a simulation on suppressing NO_x by employing evaporative compressor cooling. The results showed that the compressor performance maps (in terms of shaft power, pressure ratio, efficiency etc.) were changed due to wet compression. They modeled the evaporation rate to depend only on the mass diffusion by assuming each droplet travels with no slip with air. They also assumed all the stages were frictionless and adiabatic.

Roumeliotis and Mathioudakis [15] studied the wet compression of interstage spray with droplet heat transfer and compressor performance curve. Their results showed that the primary stages experienced unloading and the later stages were shifted to stall. They predicted a marginal increase in thermal efficiency with overspray.

They obtained the results of significant stage re-matching due to overspray. They mentioned that the behavior of different types of compressor would be different, so they suggested that the full benefit of water can be realized when a specific or similar compressor stage characteristic and geometry would be used.

Wang and Khan [3, 4] used the stage-stacking method to investigated saturated, overspray, and interstage fogging by providing the 2D compressor airfoil geometry and stage setting at the mean radius. The stage pressure ratio was enhanced during all fogging cases as did the overall pressure ratio, with saturated fogging (no overspray) achieving the highest pressure ratio. Saturated fogging reduced specific compressor work, but increased the total compressor power due to increased mass flow rate. The results of overspray and interstage spray unexpectedly showed that both the specific and overall compressor power did not reduce but actually increased. Analysis showed this increased power was contributed by increased pressure ratio and, for interstage overspray, "recompression" of "re-cooled" air contributed to more compressor power consumption. Also it was unexpected to see that air density actually decreased, rather than increased, inside the compressor with overspray. Analysis showed that overspray induced an excessive reduction of temperature that led to an appreciable reduction of pressure, so the increment of density due to reduced temperature was less than decrement of air density affected by reduced pressure as air follows the polytropic relationship. In contrast, saturated fogging resulted in increased density and reduces compressor power as expected. After the interstage spray, the local blade loading immediately showed a significantly increase. Fogging increased axial velocity, flow coefficient, blade inlet velocity, incidence angle, and tangential component of velocity.

The above study by Wang and Khan was performed with the thermal-equilibrium approach by assuming the air would reach saturation at the end of each stage as long as water droplets remained in the air. The **objectives** of this paper are to extend the previous work by including the non-equilibrium approach and compare the results between the equilibrium and non-equilibrium approaches.

STAGE-STACKING NON-EQUILIBRIUM MODEL DEVELOPMENT

Droplet Heat Transfer Model

In the non-equilibrium method the heat transfer to the droplets is calculated first to determine the droplet temperature due to surrounding heating. Then the evaporation time of the droplets will be calculated and compared with the flying time needed to pass one stage to determine if the droplets will completely evaporate at the end of the stage or not. If not, the amount of remaining liquid mass is calculated and carried to next stage.

Heat and mass transfer occur at the interface of the droplet and the surrounding air, mainly by convection and diffusion. Droplet heat transfer depends on many different parameters, e.g. slip velocity (between droplet and main fluid), temperature difference, diffusion coefficient, size (diameter) of the droplet etc. A model has been developed below to study the heat transfer of the droplets flying across each stage. A transient heat balance equation is shown in Eq.1 by treating the droplet as a lumped thermal mass with one representative temperature uniformly distributed in the droplet. The change of the droplet temperature is caused by convective and radiative heat transfer through the droplet surface. By neglecting radiative heat transfer, the droplet temperature changes as,

$$m_d Cp_d \frac{dT_d}{dt} = \pi d^2 h\left(T - T_\infty\right) \tag{1}$$

Note that liquid evaporation will reduce both liquid droplet and surrounding air temperatures. In the present model, it is assumed that the latent heat only directly affects the surrounding air temperature and the droplet temperature is predominantly affected by convection.

From Eq. (1), liquid water mass, $m_d = \rho_d \frac{1}{6}\pi d^3$

Specific heat of liquid droplet, $Cp_d = 4200$ J/kg.K

Temperature change across the rotor, $\frac{dT_d}{dt} = \frac{T_d^{i+0.5} - T_d^i}{\Delta t}$

Temperature change across the stator, $\frac{dT_d}{dt} = \frac{T_d^{i+1} - T_d^{i+0.5}}{\Delta t}$

Where, Δt = (stage length /particle velocity) which is the residence time of particle in a rotor/stator stage.

Surface area $= \pi d^2 = \frac{\frac{1}{6}\pi d^3}{\frac{1}{6}d} = \frac{V}{\frac{1}{6}d} = \frac{m_d}{\frac{1}{6}d\rho_d} = \frac{6m_d}{d\rho_d}$

Heat transfer coefficient, $h = \frac{Nuk_a}{d}$

Nusselt number, $Nu = 2 + 0.6\, Re_d^{0.5}\, Pr^{0.33}$

Droplet Reynolds number, $Re_d = \frac{\rho_d V_s d}{\mu_a}$

Slip velocity has been assumed to be 10% of air velocity according to Khan and Wang [16]. In the rotor stages, V_s is 10% of air's velocity relative to the rotor and in the stator stages, V_s is the 10% of air's absolute velocity.

Prandtl number, $Pr = \frac{\mu Cp_d}{k_a}$

Air temperature, $T_\infty = T_a = T_a^{i+0.5}$

Water temperature, $T = T_d = T_d^i$

Putting all these values in eq. (1),

$$\rho_d \tfrac{1}{6}\pi d^3 \times Cp_d \times \frac{T_d^{i+0.5} - T_d^i}{\Delta t} = \pi d^2 \frac{Nuk_a}{d}\left(T_a^{i+0.5} - T_d^i\right)$$

$$\Rightarrow \quad T_d^{i+0.5} = T_d^i + \frac{6Nuk_a\Delta t}{Cp_d\rho_d d^2}\left(T_a^{i+0.5} - T_d^i\right) \tag{2}$$

Where Δt is the residence time for air to fly passing one stage as:

$$\Delta t = \frac{L}{Vel} \tag{3}$$

Where L is the blade chord length and "Vel" is the absolute inlet velocity for stator and relative inlet velocity for the rotor.

The amount of evaporated water mass depends on evaporation, saturation pressure etc. as shown by Zheng et. al. [6], according to the Langmuir-Maxwell method [17]. Equation (4) shows the expression for the time required to evaporate the water droplet of diameter d as,

$$\tau_e = \frac{R\rho_d d^2}{8D_a\left(P_a/T_a - P_d/T_d\right)} \tag{4}$$

Where, P_d is the Saturation vapor pressure at T_d.

When, saturation pressure becomes higher than the air pressure, boiling starts and boiling time is calculated from Eq. (5), which was modified from the equation shown by Kuo [18] as,

$$\tau_b = \frac{d^2 \rho_d Cp_d}{8k_a\left(1+0.23\sqrt{Re_d}\right)\ln\left[1+\frac{Cp_d(T_a-T_d)}{h_{fg}}\right]} \quad (5)$$

For a typical environment, the value of $Cp_d\ (T_a\text{-}T_d)/\ h_{fg}$ is small (about 0.08), so $\ln[1+\ Cp_d\ (T_a\text{-}T_d)/\ h_{fg}] \approx Cp_d\ (T_a\text{-}T_d)/\ h_{fg}$. This assumption makes the eq. (5) approximately as (6),

$$\tau_b = \frac{\rho_d d^2 h_{fg}}{k_a\left(1+0.23\sqrt{Re_d}\right)(T_a-T_d)} \quad (6)$$

Empirical Formula for Water and Air Property Values

The property values of thermal conductivity, dynamic viscosity, and water vapor diffusivity in air are calculated according to Eqs. 6, 7, and 8 based on the empirical formulae in Chemistry Handbook [19]

Thermal conductivity (W/m.K), as a function of air temperature, T_a for the range of 253K to 373K

$$k_a = (46.766 + 0.7143\ T_a) \times 10^{-4} \quad (7)$$

Dynamic viscosity (Pa.s) of the air (For 273K< T_a < 373K),

$$\mu_a = (0.004823\ T_a + 0.3976) \times 10^{-5} \quad (8)$$

Mass coefficient (m^2/s) of diffusion (For 273K< Ta < 373K),

$$D_a = 2.26\times10^{-5}\left(\frac{101.325}{P_a}\right)\left(\frac{T_a}{273.15}\right) \quad (9)$$

Numerical Algorithm for Stage Performance [3, 4]

The algorithm of non-equilibrium method is built upon the previous algorithm for equilibrium method developed by Wang and Khan [3]. Since the stage-stacking algorithm and numerical procedure is comprehensive, only a brief summary of the procedure is provided below. Readers can refer [3] for detailed procedure by incorporating the non-equilibrium algorithm described in the following section in this paper.

Evaporation rate depends on relative humidity, droplet size (diameter), water vapor diffusion coefficient, heat transfer to droplet, and surrounding temperature etc. In the equilibrium method, a sufficient amount of water is allowed to evaporate to achieve saturation (100% RH) at the end of each stage until all the water evaporates, whereas in the non-equilibrium method evaporation is characterized by mass and heat transfer between air and droplet.

First, the 2-D geometries of the airfoils (stator and rotor) on the meanline and the stage setting conditions (Table A5) are selected. Based on this information, the compressor passage geometry is designed for ISO Condition (288K and 60% relative humidity) with a constant rotating speed. In the design condition, the rotor absolute inlet flow at each stage is assigned with zero absolute tangential velocity, but the relative air velocity is set equal to the blade inlet angle, i.e. no incidence angle (see Table A5).

The inlet condition at the first stage rotor is given as the static condition and the air is assumed to be saturated due to inlet fogging (Fig. 1) for both equilibrium and non-equilibrium cases. The droplet diameter is assigned uniformly at the fog sprayer first, and the droplet diameter at the compressor inlet is recalculated based on the amount of water evaporated for achieving saturation by the following equation:

$$\frac{(\dot{m}_d)_{fogger}}{(\dot{m}_d)_{inlet}} = \frac{(\rho_d)_{fogger} d^3_{fogger}}{(\rho_d)_{inlet} d^3_{inlet}} \approx \frac{d^3_{fogger}}{d_1^3} \quad (10)$$

As $(\rho_d)_{amb} \approx (\rho_d)_{inlet}$ due to incompressible nature of water.

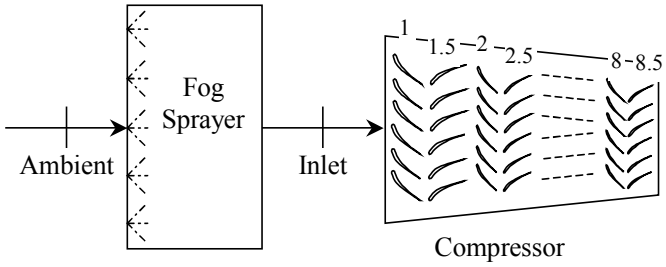

Figure 1 Calculation domain including the fog sprayer and 8-stage compressor

At the first-stage rotor inlet --- Once, the compressor inlet temperature and pressure are calculated, the total (or stagnation) status is obtained by guessing a total temperature and iterating until the total enthalpy obtained from total temperature converging to the identical value. When the ambient and inlet fogging conditions change, the air density changes and the air-water mixture mass flow rate at the first rotor inlet is calculated by assuming the compressor functions with the constant-volume-flow characteristics at the inlet (note: this is only valid at the very inlet) when the rotating speed is controlled at a constant value.

At the rotor exit, the flow is assumed to be turned at the exact angle as the blade outlet camber angle, i.e. assuming zero flow deviation angle. The status at the rotor exit is determined by matching the exit mass flow rate with the mass flow at the inlet. Two unknowns, density and absolute axial flow velocity, need to be determined during this mass flow rate matching process; therefore, two iterating loops are required. The first iteration starts by guessing the absolute axial exit velocity and drawing the velocity diagram. Iterations are conducted to ensure specific stage work obtained from the velocity diagram matches the stagnation enthalpy increase obtained from the polytropic relationship with a wet compression index of 1.36. Using the stagnation status obtained by the first iteration loop, the second iteration calculates the air-water mixture density and goes back to the first loop until the mass conservation is satisfied. Once the stagnation temperature and pressure are calculated at the rotor exit, the diameter and temperature of the droplet is calculated on the basis of heat transfer and water evaporation rate under local conditions.

Once the rotor exit parameters (pressure, density, temperature, enthalpy, etc.) are known from calculation, the **non-equilibrium parameters** (diameter of droplet, temperature of droplet, residence time etc.) are calculated as:

(i) Once the static temperature at the rotor exit is calculated in the previous step it is used as $T_a^{i+0.5}$ in Eq. (2). The droplet temperature in next stage is determined from Eq. (2) as $T_d^{i+0.5}$.

(ii) When the saturation pressure of water is less than the local static pressure and relative humidity is less than 100%, evaporation takes place and Eq. (3) is used to calculate the required

evaporation time. If the saturation pressure is higher than the local air pressure boiling takes place and Eq. (5) is used to calculate the required boiling time. If the residence time is longer than the evaporation/boiling time then water is completely evaporated before the end of this stage; otherwise, the diameter of the remaining water droplets in the next stage is calculated by taking the square root of the ratio of required evaporation/boiling time over residence time, as the evaporation is characterized by the surface area, which involves square of diameter as shown in Eq. (11).

$$\frac{d_{i+0.5}}{d_i} = \left(\frac{\Delta t}{\tau}\right)^{\frac{1}{2}} \tag{11}$$

This can be found by replacing the evaporation time with residence time in Eq (3), which gives Eq. (12)

$$\Delta t = \frac{R\rho_d d^2}{8D_a\left(P_a/T_a - P_d/T_d\right)} \tag{12}$$

(iii) Once the diameter is calculated in the next stage, the amount of survived liquid water mass can be determined from equation (13).

$$m_d = \frac{\pi}{6}\rho_d d^3 \tag{13}$$

The amount of newly evaporated water vapor is calculated by deducting this remained amount of water from the amount of water at the stage inlet. If the amount of newly calculated water vapor becomes more than the amount of water needed to saturate the air according to the local temperature and pressure, then the actually evaporated amount of water vapor is set to be the amount needed for saturation, and the actually remaining liquid water and the droplet diameter are recalculated.

The procedure for determining the second or later rotor inlet condition is different from determining the first rotor inlet status. Instead, the stagnation status (rather than the static status) at the later stage rotor inlet is known, and the static status needs to be determined. The procedure for determining the rotor exit condition is the same for all stages.

The effect of inlet or interstage fogging will change the flow coefficient and the flow inlet angle, which in turn will affect the pressure ratio and specific work of each stage.

Assumptions

1. Constant compressor inlet axial velocity (or inlet flow coefficient) -- The compressor is assumed to behave as a constant-volume-flow-rate device at the inlet when the rotating speed is controlled to be a constant value, so the inlet axial velocity remains constant. When fogging is applied, the volume flow rate at the inlet does not change although the mass flow rate increases due to increased air density. This constant volume flow assumption is based on the reason that the flow field generated by a rotating stage is determined by the blade configuration and its stage setting (staggering angle, pitch, inlet guide vane setting, etc.), so when the rotating speed maintains constant, the inlet flow filed at the first stage inlet should be almost identical. It is important to realize that the inlet velocity maintaining a constant does not mean the mass flow rate maintains constant at the inlet, nor does it mean the operation point of the first stage is the same. Once the mass flow rate is determined at the inlet, the mass flow rate maintains constant throughout the entire compressor, and the volume flow rate will change at different stages. Under increased pressure and heating due to compression, the velocity filed at first stage will be different between fogging and non-fogging conditions because both temperature and mass flow are different. This change is reflected on the increased flow coefficient (or axial velocity) at the end of the first stage.
2. The mean blade diameter was designed the same for all the stages.
3. Property values (e.g. density, enthalpy) of mixture are calculated by mass-weighted average method, similar to the process described by Young [20].
4. Equation of state (Pv = RT) holds true for all conditions.
5. The system is assumed in thermodynamic equilibrium for droplet evaporation for equilibrium cases. Water evaporation is governed by transient heat and mass transfer for non-equilibrium cases.
6. The water droplets are assumed incompressible, so the polytropic process (Pv^k = Constant) of moist air can represent the multi-phase flow. An equivalent polytropic index of 1.36 is used for moist air following the study of Klepper et al. [21]. They showed that k is approximately 1.36 for a wide range of air water mixture. Although the polytropic index may change during the course of wet compression, due to small amount of water (1-2%) is involved, k is kept at a constant value of 1.36 in this study. Variable k-values can be considered for future improvement.
7. The water droplets are assumed spherical and uniformly distributed, so they can be represented by a single-value diameter at any axial location.
8. The water droplets do not experience any break-up or coalescence.
9. The water specific heat remains constant (4200 J/kg.K).

Studied Cases

The studied compressor has 8 stages. The ISO condition (288K and 60% Relative Humidity) is used as the design case, and the diameters (hub and tip diameters) are determined at the design condition. At the designed operating condition, the axial velocity (150 m/s) is designed as a constant value throughout the compressor with the following parameters: rotor speed (12,000 RPM), rotor turning angle (12°), inlet pressure (1atm), 0.5% total pressure loss occurred in each stator and the polytropic stage efficiency (92%) is assumed for each rotor stage. A 2D compressor airfoil geometry and stage setting at the mean radii are employed. The detailed stator and rotor information are given in Table A.5 in the Appendix. Seven cases are studied with the ISO condition being the baseline (design case); one is on a hot day, one is on the same hot day with 2% overspray cooling, and the other four cases employ the same 2% overspray cooling, but use non-equilibrium heat transfer model with four different droplet diameter (arithmetic mean D_{10} = 10 μm, 15 μm, 20 μm and 30 μm for non-equilibrium cases). Note that no droplet size is involved in calculation with the equilibrium method.

Case 1: Designed baseline case at ISO condition (288K and 60% RH), no fogging.
Case 2: Under hot weather at 300K and 60% RH, no fogging.
Case 2S: Hot weather at 300K and 60% RH, saturated fogging
Case 3: 2% (wt) overspray at compressor inlet at 300K and 60% RH (equilibrium).
Case 4: Case 3 with d = 10 μm (non-equilibrium)
Case 5: Case 3 with d =15 μm (non-equilibrium)
Case 6: Case 3 with d = 20 μm (non-equilibrium)
Case 7: Case 3 with d = 30 μm (non-equilibrium)

In this study, the term "fogging" indicates the action of generating the fog. Depending on the amount of the injected water, "**saturation fogging**" implies the process of saturating the air to 100% relative humidity and "overspray" implies the process of injecting more than the water amount required to achieve saturated air. Strictly speaking, a 2% overspray implies the amount water that weighs 2% of the dry airflow is injected in addition to the amount required to saturate the air. However, for simplicity, the stated percentage of overspray fogging in this study includes both the amounts of water needed for saturation and actually oversprayed in addition to saturation. For example, 2% water overspray with an ambient condition of 300K and 60% RH implies that 0.245% water is needed to saturate the air and (2 – 0.245) = 1.755% is actually used for overspray.

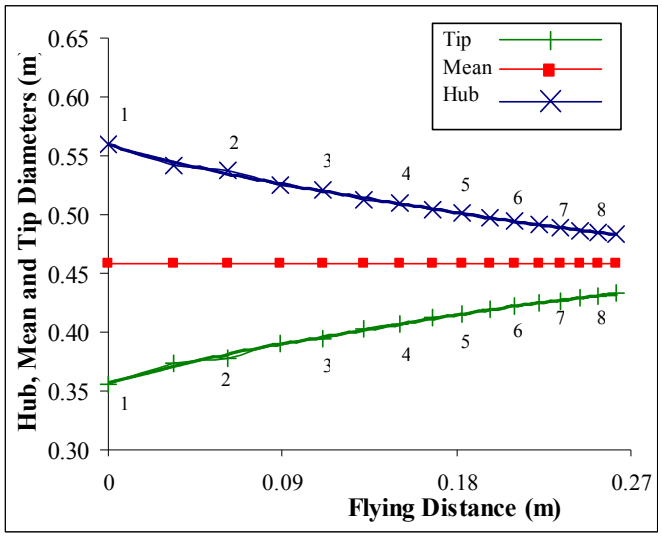

Figure 2(a) Designed compressor tip and hub diameters (the numbers on the top of the curves represent the stage numbers)

In Case 1 (design case), the axial velocity is kept as a constant in each stage by adjusting the flow area (i.e. hub and tip diameters). The variation of hub and tip diameters in different stages is shown in Fig. 2(a). For the cases of inlet fogging, the designed geometry is unchanged; the local flow velocity vector, thermal properties, rotor loading condition of each stage are calculated by the stage-stacking scheme. An example showing the effect of fogging on the velocity diagram is illustrated in Fig. 2(b) by juxtaposing the velocity diagrams of Stage 2 in Cases 1, 3 and 4 for comparison between equilibrium and non-equilibrium cases. The following differences are observed:

a. All the velocity directions and magnitudes are changed. For example, the absolute rotor inlet velocity changes from purely axial direction to deviating 0.39° for Case 2, 1.89° for Case 3, and 1.94° for Case 4 from the axis.
b. The flow coefficient ($\phi = V_a/U$) increases 2.7% for Case 2, 22.3% for Case 3 and 23.6% for Case 3.

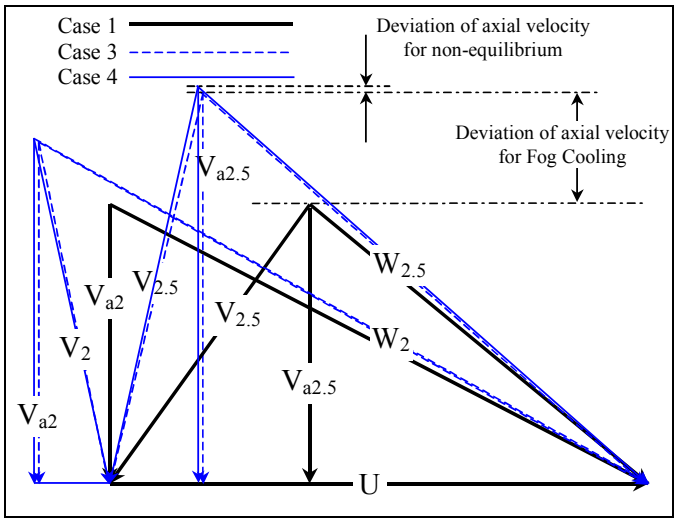

Figure 2(b) Comparison of velocity diagrams for Cases 1, 3 and 4 in second stage (V2 and W2 for Cases 3 and 4 almost coincide).

RESULTS AND DISCUSSIONS

Detailed flow physics and thermal sciences for the equilibrium cases have been explained in Wang and Khan [4]. In this paper, the discussion only focuses on the differences between employing equilibrium and non-equilibrium methods.

Droplet Size

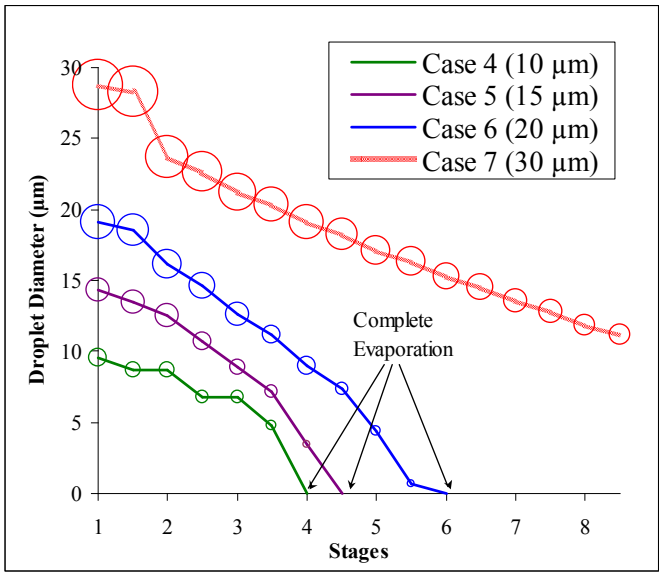

Figure 3 Reduction of droplet diameter for non-equilibrium cases

Figure 3 shows the droplet diameter variation in different stages. Droplets of all the cases evaporate completely before the compressor exit except Case 7. In general, overall evaporation of all droplets is faster in the later stages due to an increase of droplet surface area over volume ratio with smaller droplets and increase of temperature. The water in Case 7 does not complete evaporation because the residence time is short comparing to the required evaporation time. The smallest droplet diameter found for this case is 11.2 μm (Table A3).

Evaporation Rate

Evaporation rate depends on relative humidity, droplet size (diameter), water vapor diffusion coefficient, heat transfer to droplet, and surrounding temperature etc. In the equilibrium method, a sufficient amount of water is allowed to evaporate to achieve saturation (100% RH) at the end of each stage until all the water evaporates as shown in Case 3 in Fig 3. Figure 4 shows the relative humidity (evaluated at the static condition) variation along the compressor, while Fig. 5 shows the remaining liquid water in the air. The status and composition of wet air can be clearly seen from the information provided by these two figures and Table A.4. For example, in Case 3, there is sufficient water to achieve saturation until stage 3 (the third rotor); the water completely evaporates at the end of stage 3.5 (the third stator), so the relative humidity is 100% for all stages up to the third rotor. After the third stage, the relative humidity generally reduces due to increased pressure and temperature in the later stages. For example, in the beginning of the fourth stage, the pressure is 164 kPa and temperature is 339K, for which saturation vapor pressure is 25.3 kPa and 0.113 kg of water per kg of air is needed to saturate the air, but only 0.0335 kg of vapor is available which gives a 30% relative humidity.

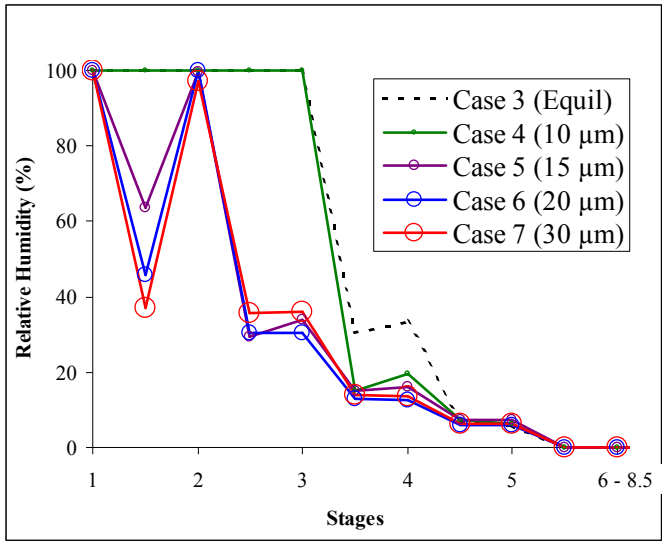

Figure 4 Variation of relative humidity for overspray cases

When non-equilibrium method is employed with the same conditions as Case 3, the result is shown as Case 4 in Fig 3. In Case 4, water evaporates completely at the end of stage 4, which is ½ stage later than Case 3. This implies that the result of using equilibrium method is very close to the non-equilibrium method for droplet size of 10 μm. However, when the droplet sizes increase, it will take longer for water to completely evaporate. Cases 5 and 6 show 15 μm and 20 μm droplets completely evaporate at stages 4.5 and 5.5, respectively. Again, droplets at 30μm do not completely evaporate at the exit of the compressor. There is about 6% (0.001kg vs. 0.0175kg) of the initial amount of water remains with the final droplet diameter at around 11.2 μm. This shows that the droplet diameter does not play any role in the equilibrium method, but significantly affect the droplet evaporation rate in the non-equilibrium method.

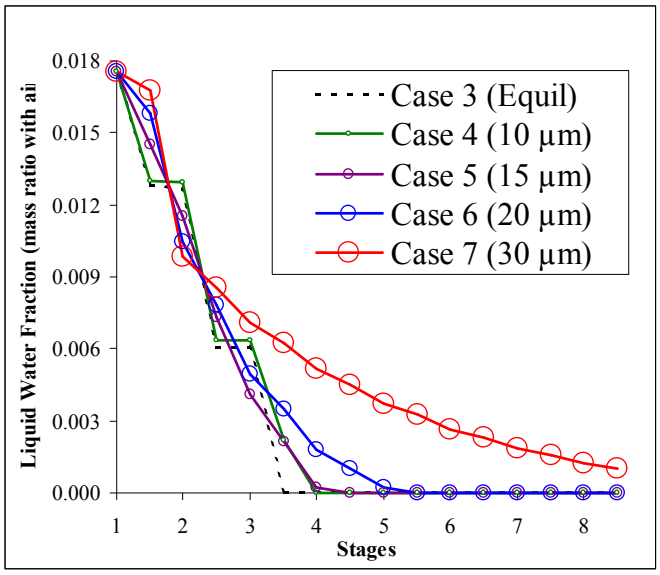

Figure 5 Variation of remaining liquid water fraction (mass ratio of water over moist air) in each stage for overspray cases

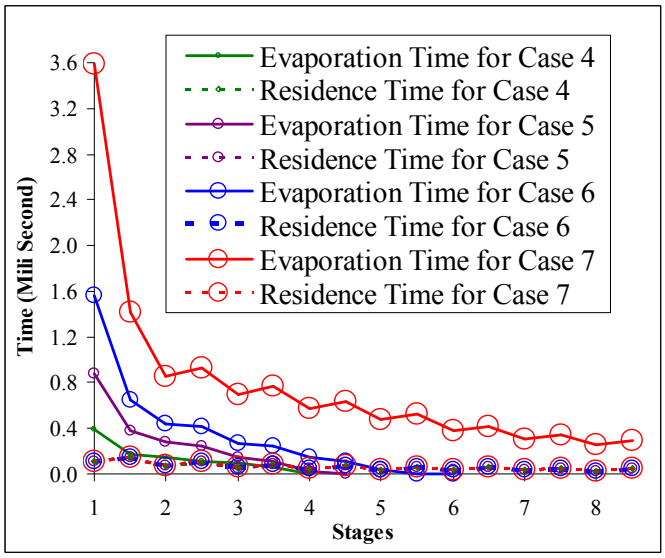

Figure 6 Residence time vs. evaporation time for non-equilibrium cases (Residence time for all four cases coincide with one another)

Evaporation of droplet is characterized by particle's aerodynamic residence time and the time required for evaporation as described in the model development. When the droplets reside inside a stage longer than the required evaporation time, all the droplets

evaporate; on the other hand, if the aerodynamic residence time is shorter than the evaporation time, droplets become smaller and fly into next stage. Figure 6 shows the aerodynamic residence time are close (between 0.1-0.2 ms) for all droplet sizes at all stages; whereas the evaporation time varies significantly with the droplet sizes, roughly in proportional to diameter square (d^2). For example, at the first stage 30 μm droplets require 3.6 ms to evaporate versus 0.4 ms for 10 μm droplets, which is 9-fold shorter.

Air and Droplets Temperature

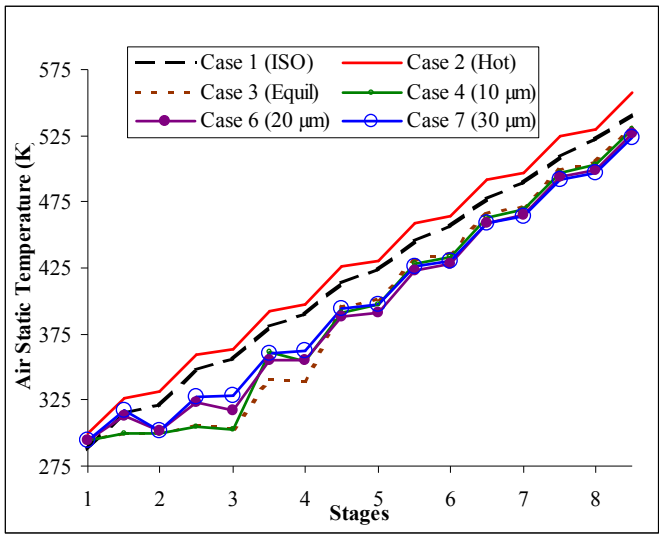

Figure 7 Air static temperature variations for all cases

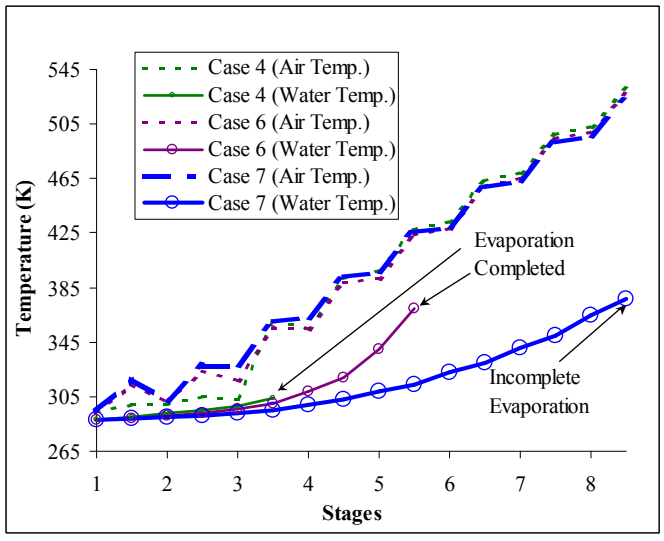

Figure 8 Air and droplet temperature variation for non-equilibrium cases

Figure 7 shows the static temperature variation in different stages for all cases. The temperature for Case 2 is higher than Case 1 in every stage. In Case 3, the temperature drops 6°C, 31°C, and 60°C in the first three stages respectively from Case 2 and maintains a relatively constant value for the first three stages before the completion of evaporating all the water droplets. Non-equilibrium method (Case 4) results in a very similar evaporation and temperature reduction as equilibrium method (Case 3) except between stages 3 and 4 where the liquid completely evaporates in Case 3 but not in Case 4. Cases 6 and 7 have slower evaporation, which makes air temperature reduction less in the earlier four stages, but once all water evaporates and the vapor is superheated downstream of stage 4.5, the curves for equilibrium and all non-equilibrium cases are almost coincided to one another, except Case 7 has a bit lower temperature due to its unfinished evaporation.

Figure 8 shows the droplet temperature variation and the difference between droplet and air temperatures. It is interesting to notice that the droplet temperature never catches up with the air temperature.

Velocity

In the design case (Case 1), the axial velocity, flow coefficient ($\Phi=V_{ax}/U$) and the inlet velocity at each rotor inlet is designed as the same value throughout the compressor by changing the air passage cross-sectional area to satisfy mass conservation. However, when fogging is applied, the air velocity increases significantly and then falls off to the values without fogging after water droplets completely evaporate. The variation of inlet velocity at each stage is shown in Fig. 9(a). Cases 1 and 2 only differ at the ambient temperature, so their inlet velocities follow a similar variation trend with Case 2's inlet velocities a bit higher. Significant increase of velocity occurs in stages 2 to 5 when fogging is applied in Cases 3 and 4. Both cases reach a peak velocity of 250 m/s at stage 3 rotor inlet. The only major difference between Cases 3 and 4 is at stage 4 where equilibrium method (Case 3) predicts a complete liquid evaporation showing a continuous high velocity; whereas, Case 4 predicts only partial liquid evaporation with less temperature reduction and less velocity increase.

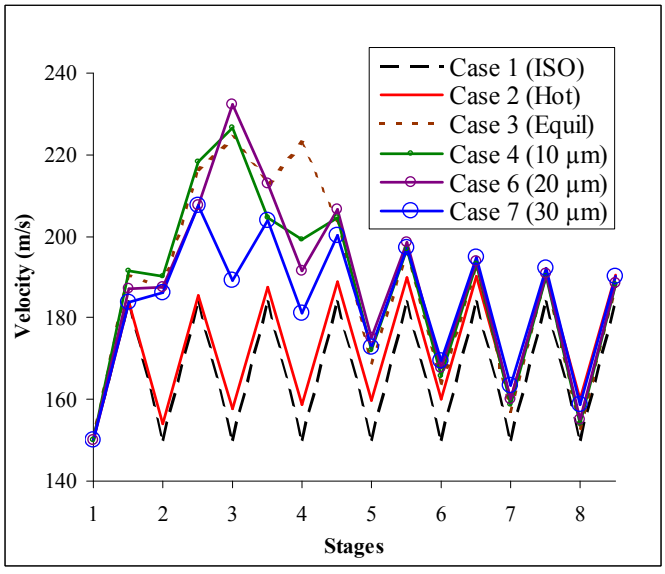

Figure 9 (a) Inlet velocity variations for all cases

As the temperature drops due to fogging in Cases 3 and 4 (Fig. 7) the static pressure also drops from Stages 2 to 5 (Fig. 10), which results in a reduction of density and an increase in axial velocity to conserve the mass. This is also reflected in the flow coefficient

increase in Fig. 9b. On the other hand, due to slower evaporation of larger droplets in Cases 6 and 7, temperature does not have any sudden drop, so these two cases have less drastic changes in velocity and flow coefficient. Overall speaking, all the fogging cases (Cases 3-7) have higher flow coefficients until 7th stage; afterwards their flow coefficients drop below Case 2. This behavior is consistent with the results obtained by White and Meacock [22], where they showed that the flow coefficient (ϕ) increases till third stage and then decreased and eventually got lower than the dry compression values.

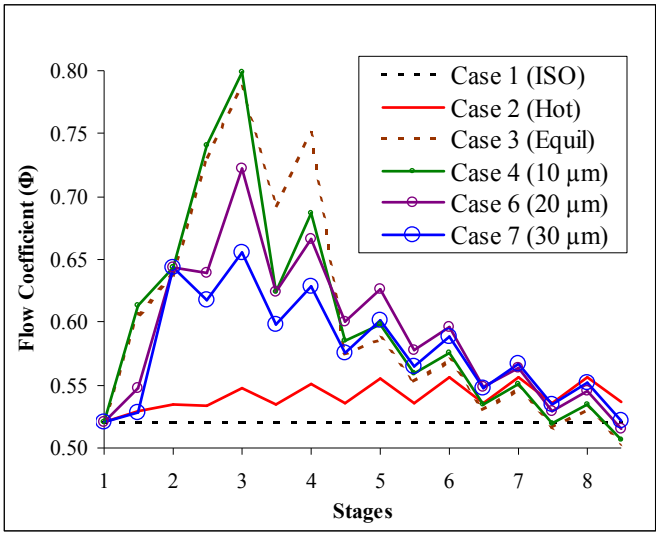

Figure 9 (b) Flow coefficient variations for all cases

Combining the information obtained in Figs. 7 and 9, the results show that the flow coefficient must significantly increase to accommodate more mass flow rate contributed by overspray especially when the air (not air-liquid mixture) density reduces, as shown in Fig. 10, rather than increases after overspray is applied. The trend of decreased air density with overspray fogging seems counter-intuitive initially, but this phenomenon has specifically explained by Wang and Khan [3, 4]. They explained that when overspray is applied, temperature drops significantly (70-90^{o}C) due to water evaporation. This excessive temperature reduction results in a significant reduction in pressure. Pressure usually reduces more than the temperature as it can be seen from the polytropic relation that $PT^{k/(k-1)}$ = Constant, i.e. $P \propto T^{(k-1)/k}$. Take k = 1.36 for moist air for example, so k/(k-1) = 3.78, which means if the temperature (absolute value) reduces 10%, the pressure will reduce 30%. Based on the ideal gas law $\rho \sim P/RT$, the density reduces instead of increasing. Although the air receives more water vapor when water droplets vaporize, the slightly increased density due to water evaporation is not large enough to compensate for the density reduction due to temperature-induced pressure reduction. Eventually, the air density of oversprayed cases becomes denser than non-fogging case after stage 6.5. This density variation trend due to overspray fogging is also in agreement with the results White and Meacock [22] and Roumeliotis and Mathioudakis [15]. Note that the air density of saturated fogging case (Case 2S) will always be higher than non-fogging case as have been shown in [4] because no wet-compression and no water evaporation occurs inside the compressor.

Pressure Ratio

The static pressure distributions are shown in Fig. 10. Saturated fogging (Case 2S) increases static pressure as expected, while overspray reduces the local static pressure due to continuous water evaporation inside the compressor. Equilibrium method (Case 3) results in lower static pressure between stages 3 and 4, but ends up with a little higher pressure than non-equilibrium cases.

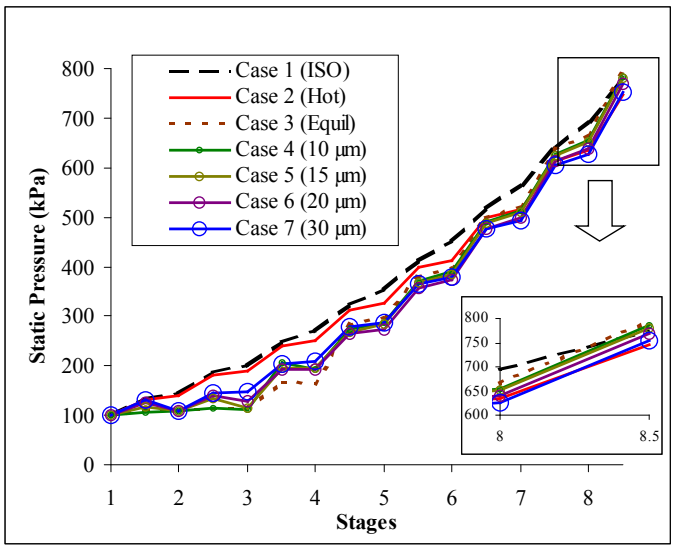

Figure 10 Stage static pressure variation for all cases

Figures 13a and 13b show the local and accumulative stagnation pressure ratios. Again, Case 2S (saturated fogging) is shown to achieve the highest overall stagnation pressure ratio (8.54), which is noticeably above the stagnation pressure ratio from non-equilibrium Cases 4, 5, 6 and 7 with the values of 7.63, 7.58, 7.48 and 7.33, respectively (see Fig. 13b or Table A2).

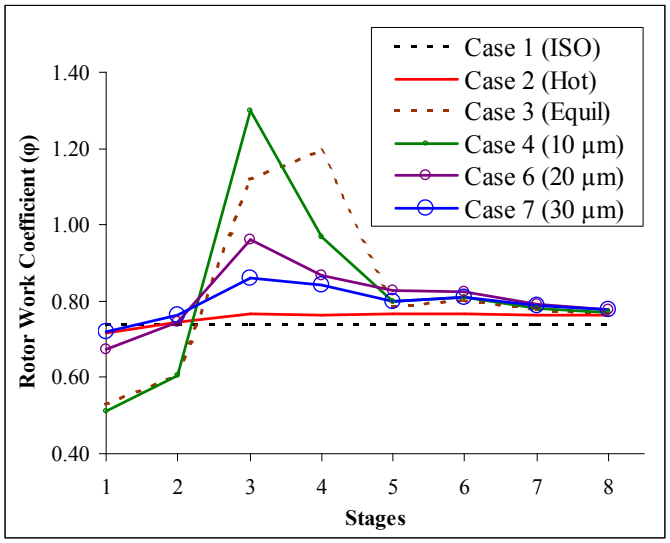

Figure 11 Rotor Work Coefficient variation for all cases

For Case 2, when ambient is hot, the local stagnation pressure ratio at the first stage drops from 1.396 of the ISO condition (Case 1)

to 1.366. At the last stage, the local stagnation pressure ratio of Case 2 is 1.206 versus 1.208 of Case 1. When fogging is applied in Case 3, the local stagnation pressure ratio experiences a significant drop from 1.4 to 1.0 at the first stage due to reduced temperature, but the local stagnation pressure ratios of Stags 2-4 immediately rise above 1.6, indicating the rotors of these two stages work very hard as evidenced in their high work coefficients (ψ) shown in Fig. 11. Not until the fifth stage, does the local stagnation pressure ratio of Case 3 reduce to a level around 1.32, which is about 5% higher than Case 1.

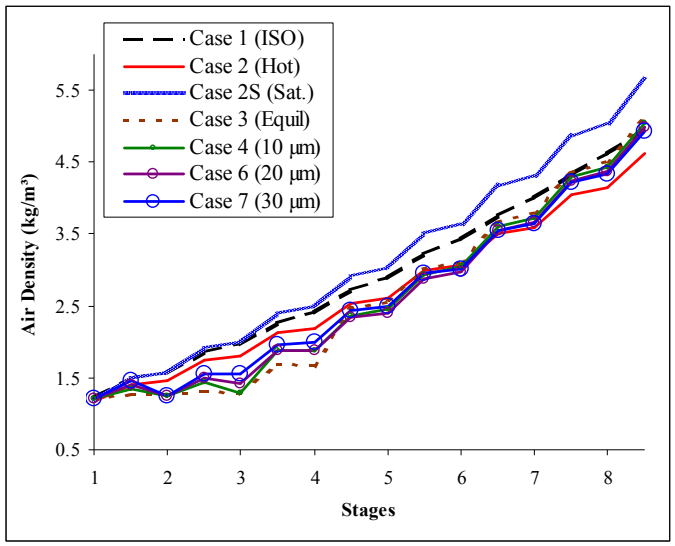

Figure 12 Moist Air density variation for all cases

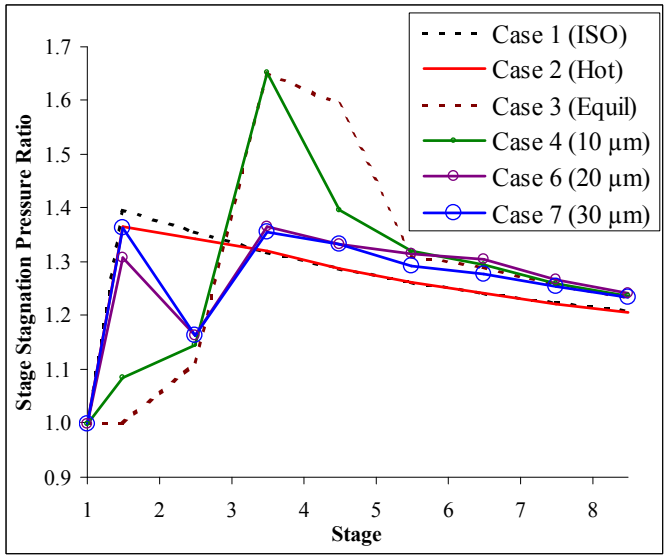

Figure 13(a) Stage overall stagnation pressure ratio variation for all cases

When non-equilibrium method is applied in Case 4, the local stagnation pressure ratio is higher than those calculated by equilibrium method in Case 3 at stages 1-3. An obvious difference between Case 3 and 4 (or equilibrium versus non-equilibrium approaches) is between Stage 3 and 4 where all liquid is predicted completely evaporated in Cases 3 but not yet in Case 4. This difference results in more cooling, lower static temperature (Fig. 7), lower static pressure (Fig. 10), and lower density (Fig. 12) in Case 3, but higher local stagnation pressure ratio between stages 3.5 and 5 than in Case 4. More liquid evaporated accompanied with low overall density leads to more volume flow rate and hence higher inlet velocity (Fig. 9a) and flow coefficient (Fig. 9b) for Case 3 between stages 3.5 and 4.

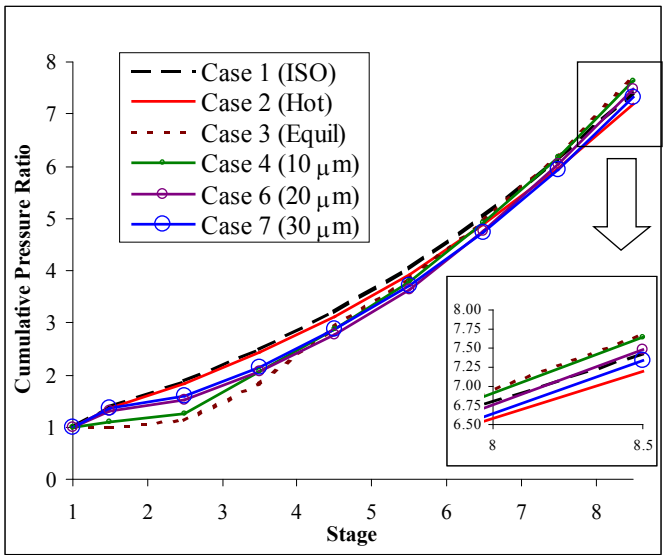

Figure 13(b) Cumulative overall stagnation pressure ratio variation for all cases

Compressor Power

The required compressor power (MW) is shown in Fig. 14 and the specific work (kW/(kg/s) = kJ/kg) in P-v diagram is shown in Fig. 15. In contrast to saturated fogging which actually reduces compressor power, overspray (Cases 3 versus Case 2) increases both specific compressor work by 8.65% due to increased pressure ratio and the total compressor power by 12.6% due to increased mass flow rate. This seemingly counter-intuition phenomenon was explained in detail in the previous paper [4] and is not repeated here. Basically, overspray increases stagnation pressure ratio and the compressor work increases, which can be represented by the area on the left of the compression curve on the P-v diagram.

The specific work for Case 3 (272 kJ/kg) is very close to Case 4 (271 kJ/kg). The total powers for both cases are also very close (7.909 MW vs. 7.873 MW) because their mass flow rates are identical (26.71 kg/s) as shown in Table 1. As the diameter increases from 10 μm to 30 μm, the specific work decreases from 271 to 263 kJ/kg. Since less power is used to produce less pressure ratio, a fair way to compare the compressor performance is to compare the compressor power per unit increase of pressure ratio (W_c/P_r) in Table 1. As it can be seen, equilibrium method (Case 3) predicts more efficient compression with W_c/P_r = 1028 kW than non-equilibrium Case 4 with W_c/P_r = 1031 kW by assuming instantaneous water evaporation. Case 2S, having achieved W_c/P_r = 830 kW, is the most effective in all cases due to its complete evaporation before compression. This fact is revealed in Fig. 15, which shows the P-v curve of Case 2s is situated at the leftmost of all the curves and requires the least amount of specific work (248 kJ/kg) among all cases, although it produces the highest stagnation pressure ratio (8.54). Among the four non-equilibrium cases, Case 4 with 10 μm (smallest droplet) is most effective among the 4 non-equilibrium cases and Case 7 (30 μm droplet) is the least effective.

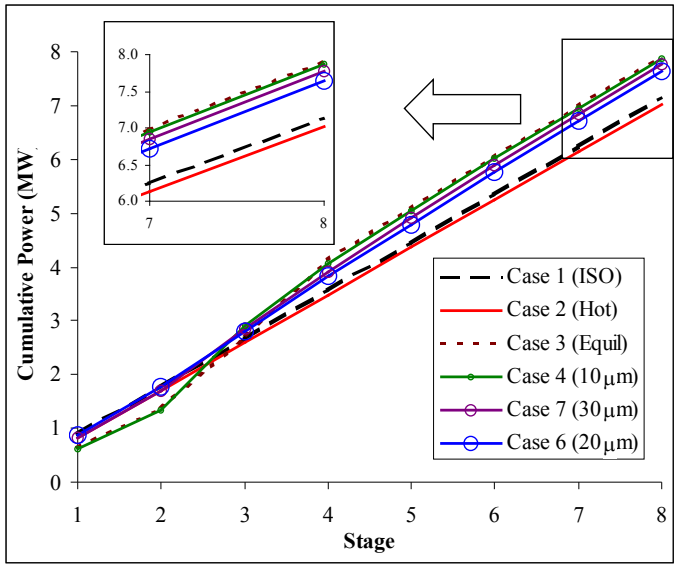

Figure 14 Cumulative total compressor power variation for all cases

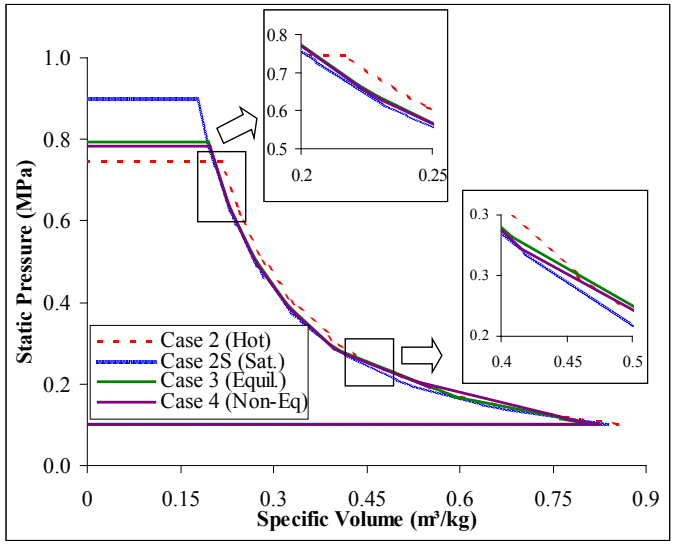

Figure 15 P-v diagram to show specific work for four cases

The present result of increased compressor power consumption due to wet compression is consistent with Bagnoli et. al. [23], Roumeliotis and Mathioudakis [24], Williams [25] and Wang and Khan [3, 4], but inconsistent with Abdelwahab [11] and Sanaye et. al. [12]. Although White and Meacock [22] showed compressor power reduced with fogging, their presentation could be misleading without looking into their assumption and practice. Their analysis indeed showed that the compression with fogging produces more pressure ratio than the dry compression. However, when the comparison was made, they didn't compare the actual compressor power consumptions corresponding to the different pressure ratios of each case, rather they jacked up the pressure ratio of the dry compression to equal the wet compression pressure ratio, which of course led to the conclusion that wet compression required less power.

Table 1 Overall compressor performance and net gas turbine output power

Cases	Mass flow rate (kg/s)	Specific Work (kJ/kg)	Comp. Power (MW)	P_r	Comp. Power /P_r (kW)	Net GT Output (MW)
1	26.91	244	7.139	7.42	962	8.609
2	25.77	251	7.024	7.20	975	7.904
2S	26.25	248	7.088	8.54	830	8.357
3	26.71	272	7.909	7.69	1028	9.039
4	26.71	271	7.873	7.63	1031	9.057
5	26.71	270	7.838	7.57	1035	8.971
6	26.71	268	7.780	7.48	1040	8.912
7	26.71	263	7.647	7.34	1042	8.912

It is encouraging to know that the present results are supported by the recent experimental results from Roumeliotis and Mathioudakis [24]. They showed that the compressor power increased by water injection and the increased compressor power was linear with the quantity of water entering the stage. As a result, the compressor isentropic efficiency decreases linearly with the amount of water injected.

Although the compressor power consumption increases in the saturated fogging and overspray cases, the total gas turbine net power increases nonetheless as shown in Table 1.

SUMMARY

This paper compares the results of thermal equilibrium and non-equilibrium methods for overspray fogging through stag-stacking scheme with given mean-line blade and 8-stage compressor configurations. The results are summarized below:

1. Saturated fogging achieves highest pressure ratio augmentation and reduces compressor power consumption; whereas overspray actually increases both the specific and overall compressor power for both equilibrium and non-equilibrium cases. Nevertheless, the net GT power output increases with both saturated and overspray fogging.

2. Non-equilibrium method differs from the equilibrium method due to the change of evaporation rate. Droplet size doesn't play a role in equilibrium approach, but plays a major role in affecting the result in the non-equilibrium case. For small droplet size of 10 μm, the droplet evaporation rate is fast, so the non-equilibrium method predicts close results as the equilibrium method. Larger droplets lead to slower evaporation, reduction of pressure ratio, and less effective compressor performance than the smaller droplets.

3. Equilibrium method predicts that wet compression increases axial velocity, blade inlet velocity, incidence angle, and tangential component of velocity. Non-equilibrium methods predict a similar trend except with lesser increments as the droplet size increases.

4. In the present study, the equilibrium method predicts that all the water droplets evaporate completely at the end of stage 3, while the non-equilibrium approach predicts that the completion of evaporation delays; but all droplets completely evaporate in the

compressor except approximately 10% of the biggest droplets (30μm) escape from the compressor.

5. Saturated fogging increases air density; however, both equilibrium and non-equilibrium methods predict that wet compression actually reduces air density in the earlier 70% of the compressor.

6. Non-equilibrium predicts small droplets relax the load in the earlier stages, but increases the load in the later stages. Larger droplets show less load changes.

ACKNOWLEDGEMENT

This study was supported by the Louisiana Governor's Energy Initiative via the Clean Power and Energy Research Consortium (CPERC) and administered by the Louisiana Board of Regents.

REFERENCES

1. Meher-Homji, C.B. and Mee, T.R., 1999, "Gas Turbine Power Augmentation by Fogging of Inlet Air," Proceedings of 28th Turbomachinery Symposium, Houston, Texas, USA, September 1999.
2. Bagnoli, M., Bianchi, M., Melino, F., Peretto, A., Spina, P.R., Bhargava, R. and Ingistov, S., 2004, "A Parametric Study of Interstage Injection on GE Frame 7EA Gas Turbine," Proceedings of ASME Turbo Expo 2004, Vienna, Austria, June 14-17, ASME Paper No: GT-2004-53042.
3. Wang, T. and Khan, J. R., 2008, "Overspray and Interstage Fog Cooling in Compressor using Stage-Stacking Scheme -- Part 1: Development of Theory and Algorithm", Proceedings of ASME Turbo Expo 2008, Berlin, Germany, June 9-13, 2008, ASME Paper No: GT-2008-50322.
4. Wang, T. and Khan, J. R., 2008, "Overspray and Interstage Fog Cooling in Compressor using Stage-Stacking Scheme -- Part 2: Case Study," Proceedings of ASME Turbo Expo 2008, Berlin, Germany, June 9-13, 2008, ASME Paper No: GT-2008-50323.
5. Hill P. G., "Aerodynamic and Thermodynamic Effects of Coolant Injection on Axial Compressors," Aeronautical Quarterly, February 1963, pp. 333-348.
6. Zheng, Q., Sun, Y., Li, S. and Wang, Y, 2002, "Thermodynamic Analysis of Wet Compression Process in the Compressor of Gas Turbine," Proc. of ASME Turbo Expo 2002, Amsterdam, The Netherlands, June 3-6, ASME Paper No: GT-2002-30590.
7. Zheng, Q., Li, M., Sun, Y., 2003, "Thermodynamic Analysis of Wet Compression and Regenerative (WCR) Gas Turbine," Proceedings of ASME Turbo Expo 2003, Atlanta, Georgia, USA, June 16-19, ASME Paper No: GT-2003-38517.
8. Khan, J. R. and Wang, T., 2006, "Fog and Overspray Cooling for Gas Turbine Systems with Low Calorific Value Fuels," Proceedings of ASME Turbo Expo 2006, Barcelona, Spain, May 8-11, 2006, ASME Paper No: GT-2006-90396.
9. Williams, J., "Further Effects of Water Ingestion on Axial Flow Compressors and Aeroengines at Part Speed," Proceedings of ASME Turbo Expo 2008, Berlin, Germany, June 9-13, 2008, ASME Paper No: GT2008-50620.
10. Payne, R.C. and White, A.J., 2007, "Three-Dimensional Calculations of Evaporative Flow in Compressor Blade Rows," Proceedings of ASME Turbo Expo 2007, Montreal, Canada, May 14-17, 2007, ASME Paper No: GT-2007-27331.
11. Abdelwahab, A., 2006, "An Investigation Of The Use Of Wet Compression In Industrial Centrifugal Compressors," Proceedings of ASME Turbo Expo 2006, Barcelona, Spain, May 8-11, 2006, ASME Paper No: GT-2006-90695.
12. Sanaye, S., Rezazadeh, H., and Aghazeynali, M., 2006, "Effects of Inlet Fogging and Wet Compression on Gas Turbine Performance," Proceedings of ASME Turbo Expo 2006, Barcelona, Spain, May 8-11, 2006, ASME Paper No: GT-2006-90719.
13. Bianchi, M., Melino, F., Peretto, A., Spina, P.R. and Ingistov S., 2007, "Influence of Water Droplet Size and Temperature on Wet Compression," Proceedings of ASME Turbo Expo 2007, Montreal, Canada, May 14-17, 2007, ASME Paper No: GT-2007-27458.
14. Sexton, M. R., Urbach, H. B., Knauss, D. T., 1998 "Evaporative Cooling for NOx Suppression and Enhanced Engine Performance for Naval Gas Turbine Propulsion Plants," ASME paper 98-GT-332.
15. Roumeliotis I., Mathioudakis K., 2006, "Evaluation of Interstage Water Injection Effect on Compressor and Engine Performance," ASME Journal of Engineering for Gas Turbine and Power, Paper GTP-05-1123, Vol. 128/4, pp. 849-856, also ASME paper 2005-GT-68698.
16. Khan, J. R. and Wang, T., 2008, "Simulation of Inlet Fogging and Wet-compression in a Single Stage Compressor Including Erosion Analysis," Proceedings of ASME Turbo Expo 2008, Berlin, Germany, June 9-13, 2008, ASME Paper No: GT-2008-50874.
17. Chai, Y. 1995, "Two-Phase Flows in Steam Turbine," Xi'an Jiaotong University Press.
18. Kuo, K. K. Y., "Principles of Combustion," John Wiley and Sons, New York, 1986.
19. Handbook Of Chemistry, CRC Press, 59th Edition.
20. Young J. B., "The Fundamental Equations of Gas-Droplet Multiphase Flow," Int. J. Multiphase Flow, Vol. 21, No. 2, pp.175-191, 1995.
21. Klepper J., Hale A., Davis M., Hurwitz W., "A Numerical Investigation of the Effects of Steam Ingestion on Compression System Performance," ASME paper No. GT2004-54190.
22. White A. J., Meacock A J., 2004, "An evaluation of the effects of water injection on compressor performance," ASME J. of Engineering for Gas Turbines and Power, Vol. 126, pp.748-754.
23. Bagnoli, M., Bianchi, M., Melino, F. and Spina, P.R., 2006, "Development and Validation of a Computational Code for Wet Compression Simulation of Gas Turbines," Proceedings of ASME Turbo Expo 2006, Barcelona, Spain, May 8-11, 2006, ASME Paper No: GT-2006-90342.
24. Roumeliotis, I. and Mathioudakis, K., 2007, "Water Injection Effects on Compressor Stage Operation," ASME Journal of Engineering for Gas Turbines and Power, Vol. 129, pp. 778-784.
25. Williams, J., 2008, "Further Effects of Water Ingestion on Axial Flow Compressors and Aeroengines at Part Speed", Proceedings of ASME Turbo Expo 2008, Berlin, Germany, June 9-13, ASME Paper No: GT-2008-50620.

APPENDIX

Table A1 Detailed stage-stacking data (pressures, temperature, velocity, flow coefficient, Mach numbers and density) for all cases. (Shaded areas represent the stator stages and the non-shaded rows represent rotor stages.)

Stage	Total Pressure (kPa)						
	Case 1	Case 2	Case 3	Case 4	Case 5	Case 6	Case 7
1	115.6	115.1	115.7	115.7	115.7	115.7	115.7
1.5	161.6	157.4	115.7	125.6	142.5	151.6	158.0
2	161.4	157.2	115.7	125.6	142.4	151.4	157.8
2.5	218.9	211.5	128.7	143.9	168.3	176.3	183.9
3	218.6	211.2	128.6	143.8	168.1	176.2	183.7
3.5	288.5	279.0	212.9	250.6	243.1	240.9	249.5
4	288.1	278.6	212.5	250.0	242.8	240.5	249.2
4.5	371.4	358.9	339.1	330.2	325.8	321.1	332.6
5	371.0	358.5	338.5	329.8	325.4	320.7	332.2
5.5	468.9	453.0	444.5	436.1	432.4	422.4	429.7
6	468.4	452.5	443.9	435.5	431.9	421.9	429.2
6.5	582.0	562.5	574.0	565.1	561.3	551.1	549.4
7	581.4	561.9	573.3	564.5	560.7	550.4	548.8
7.5	711.6	687.5	721.8	712.7	708.8	698.1	688.7
8	710.9	686.9	721.1	712.0	708.0	697.3	688.0
8.5	859.2	829.1	891.0	881.3	877.2	866.1	850.1

Stage	Static Pressure (kPa)						
	Case 1	Case 2	Case 3	Case 4	Case 5	Case 6	Case 7
1	101.3	101.3	101.3	101.3	101.3	101.3	101.3
1.5	134.9	132.2	108.5	107.2	117.0	125.6	131.5
2	144.7	139.3	108.7	107.3	107.7	108.4	108.7
2.5	185.8	180.0	115.7	113.9	132.9	139.9	146.2
3	201.9	188.4	113.3	111.3	114.4	129.0	146.7
3.5	248.4	240.1	167.9	205.3	193.9	193.1	203.6
4	271.4	250.7	164.1	191.5	193.9	193.0	207.9
4.5	323.8	312.2	281.4	272.1	267.9	264.1	277.8
5	354.3	325.0	298.5	288.3	283.1	272.2	286.6
5.5	413.1	397.8	379.9	371.2	367.5	357.2	366.3
6	451.7	413.1	398.2	388.9	384.9	373.8	378.2
6.5	517.3	498.2	499.3	490.4	486.6	476.2	475.6
7	564.6	516.2	522.6	513.2	509.2	498.3	493.2
7.5	637.7	613.7	636.2	627.2	623.4	612.8	604.1
8	694.1	634.3	664.9	655.1	650.9	639.5	627.0
8.5	775.4	745.8	794.2	784.4	780.3	769.2	753.8

Stage	Static Temperature (K)						
	Case 1	Case 2	Case 3	Case 4	Case 5	Case 6	Case 7
1	288.0	300.0	294.2	294.2	294.2	294.2	294.2
1.5	315.2	326.3	299.5	299.2	307.1	313.3	317.5
2	321.5	331.2	299.7	299.3	300.4	301.4	301.9
2.5	348.0	358.9	305.4	305.0	318.8	323.5	327.7
3	356.4	363.6	303.8	303.2	306.4	316.7	328.0
3.5	380.7	392.4	341.0	361.0	355.4	354.9	360.2
4	390.4	397.3	339.0	354.4	355.4	354.9	362.2
4.5	413.2	425.7	395.2	391.5	389.7	388.1	393.7
5	424.0	430.6	401.4	397.5	395.5	391.3	397.0
5.5	445.6	458.9	430.6	427.8	426.6	423.1	426.1
6	457.1	463.9	436.0	433.1	431.8	428.2	429.7
6.5	477.8	492.0	465.6	463.3	462.2	459.4	459.2
7	489.9	497.0	471.3	468.8	467.8	465.0	463.7
7.5	509.8	524.8	499.1	497.1	496.2	493.8	491.8
8	522.3	529.8	505.0	502.9	501.9	499.4	496.7
8.5	541.6	557.5	531.9	530.0	529.2	527.1	524.0

Stage	Density (kg/m^3)						
	Case 1	Case 2	Case 3	Case 4	Case 5	Case 6	Case 7
1	1.222	1.170	1.213	1.213	1.213	1.213	1.213
1.5	1.488	1.405	1.268	1.255	1.337	1.409	1.458
2	1.564	1.458	1.269	1.256	1.253	1.255	1.256
2.5	1.856	1.738	1.314	1.296	1.448	1.503	1.553
3	1.969	1.795	1.294	1.275	1.292	1.411	1.554
3.5	2.268	2.120	1.694	1.879	1.883	1.881	1.961
4	2.416	2.187	1.666	1.818	1.879	1.876	1.989
4.5	2.719	2.535	2.450	2.406	2.365	2.344	2.442
5	2.899	2.608	2.559	2.508	2.463	2.395	2.497
5.5	3.216	2.993	3.009	2.974	2.939	2.881	2.948
6	3.428	3.075	3.115	3.077	3.040	2.978	3.014
6.5	3.759	3.501	3.669	3.634	3.599	3.542	3.551
7	4.001	3.591	3.793	3.758	3.724	3.667	3.648
7.5	4.342	4.041	4.357	4.326	4.295	4.244	4.211
8	4.613	4.137	4.500	4.466	4.432	4.377	4.324
8.5	4.970	4.623	5.108	5.074	5.042	4.990	4.924

Stage	Inlet Velocity (m/s)						
	Case 1	Case 2	Case 3	Case 4	Case 5	Case 6	Case 7
1	150.0	150.0	150.0	150.0	150.0	150.0	150.0
1.5	183.7	184.0	190.6	191.4	187.2	184.9	183.9
2	150.0	154.1	187.5	190.1	187.7	185.9	186.1
2.5	183.7	185.6	216.0	218.2	207.4	207.4	207.5
3	150.0	157.6	223.9	226.8	232.3	209.6	189.2
3.5	183.7	187.6	213.3	204.4	213.0	210.8	204.0
4	150.0	158.6	222.7	199.2	191.6	192.1	181.0
4.5	183.7	188.9	203.4	204.5	206.7	206.1	200.2
5	150.0	159.7	168.7	172.1	175.3	180.3	172.9
5.5	183.7	189.8	195.7	196.9	198.4	200.6	197.1
6	150.0	160.1	163.9	165.9	167.9	171.4	169.4
6.5	183.7	190.3	192.2	193.0	194.0	195.5	194.8
7	150.0	160.0	157.2	158.6	160.0	162.5	163.3
7.5	183.7	190.4	189.5	190.1	190.7	191.7	192.3
8	150.0	160.1	152.9	154.0	155.1	157.0	158.9
8.5	183.7	190.5	187.5	188.0	188.5	189.4	190.3

Stage	Absolute Mach Number						
	Case 1	Case 2	Case 3	Case 4	Case 5	Case 6	Case 7
1	0.440	0.431	0.439	0.439	0.439	0.439	0.439
1.5	0.515	0.507	0.551	0.553	0.535	0.523	0.518
2	0.417	0.421	0.541	0.549	0.541	0.535	0.534
2.5	0.491	0.487	0.615	0.622	0.579	0.575	0.572
3	0.396	0.411	0.639	0.713	0.660	0.586	0.520
3.5	0.469	0.471	0.573	0.527	0.561	0.556	0.535
4	0.378	0.396	0.6	0.510	0.504	0.506	0.473
4.5	0.450	0.455	0.507	0.516	0.519	0.519	0.502
5	0.363	0.382	0.417	0.430	0.437	0.452	0.431
5.5	0.433	0.440	0.466	0.472	0.474	0.482	0.473
6	0.349	0.369	0.387	0.395	0.399	0.409	0.404
6.5	0.418	0.426	0.44	0.444	0.446	0.451	0.450
7	0.337	0.357	0.358	0.363	0.366	0.373	0.375
7.5	0.405	0.413	0.419	0.422	0.423	0.426	0.429
8	0.327	0.346	0.336	0.340	0.342	0.347	0.353
8.5	0.393	0.401	0.402	0.404	0.405	0.408	0.411

Stage	Relative Mach Number						
	Case 1	Case 2	Case 3	Case 4	Case 5	Case 6	Case 7
1	0.953	0.932	0.949	0.949	0.949	0.949	0.949
1.5	0.661	0.659	0.793	0.802	0.744	0.700	0.672
2	0.902	0.899	1.078	1.089	1.048	1.012	0.991
2.5	0.629	0.628	0.905	0.918	0.784	0.736	0.699
3	0.857	0.862	1.245	1.264	1.150	1.056	0.979
3.5	0.602	0.595	0.78	0.655	0.655	0.665	0.650
4	0.818	0.822	1.087	0.940	0.928	0.938	0.908
4.5	0.577	0.568	0.59	0.602	0.609	0.620	0.605
5	0.785	0.787	0.823	0.838	0.848	0.866	0.845
5.5	0.556	0.545	0.56	0.567	0.571	0.580	0.574
6	0.756	0.757	0.781	0.790	0.794	0.806	0.801
6.5	0.537	0.525	0.525	0.530	0.533	0.539	0.541
7	0.730	0.731	0.735	0.741	0.744	0.753	0.756
7.5	0.520	0.508	0.499	0.503	0.505	0.510	0.515
8	0.707	0.708	0.7	0.705	0.707	0.713	0.720
8.5	0.504	0.493	0.477	0.480	0.482	0.486	0.492

Stage	Flow Coefficient (Φ)						
	Case 1	Case 2	Case 3	Case 4	Case 5	Case 6	Case 7
1	0.521	0.521	0.521	0.521	0.521	0.521	0.521
1.5	0.521	0.529	0.607	0.613	0.576	0.547	0.528
2	0.521	0.535	0.637	0.644	0.646	0.644	0.644
2.5	0.521	0.533	0.731	0.741	0.663	0.639	0.618
3	0.521	0.547	0.787	0.799	0.789	0.722	0.655
3.5	0.521	0.534	0.692	0.624	0.623	0.624	0.598
4	0.521	0.551	0.750	0.687	0.665	0.666	0.628
4.5	0.521	0.536	0.574	0.585	0.595	0.600	0.576
5	0.521	0.555	0.586	0.598	0.609	0.626	0.601
5.5	0.521	0.536	0.553	0.559	0.566	0.578	0.565
6	0.521	0.556	0.569	0.576	0.583	0.596	0.588
6.5	0.521	0.536	0.530	0.535	0.540	0.549	0.548
7	0.521	0.556	0.546	0.551	0.556	0.564	0.567
7.5	0.521	0.536	0.516	0.519	0.523	0.529	0.534
8	0.521	0.556	0.530	0.534	0.538	0.545	0.552
8.5	0.521	0.537	0.503	0.507	0.510	0.515	0.522

Table A2 Detailed stage-stacking data (pressure ratio, power, rotor work coefficient, de Haller number) for all cases

Stage	Stage Pressure Ratio						
	Case 1	Case 2	Case 3	Case 4	Case 5	Case 6	Case 7
1	1.396	1.366	1.000	1.085	1.231	1.308	1.364
2	1.355	1.344	1.112	1.146	1.181	1.164	1.164
3	1.318	1.319	1.651	1.652	1.444	1.365	1.356
4	1.288	1.287	1.593	1.395	1.341	1.333	1.333
5	1.263	1.262	1.311	1.321	1.327	1.316	1.292
6	1.241	1.242	1.291	1.295	1.298	1.305	1.278
7	1.223	1.222	1.258	1.260	1.263	1.267	1.254
8	1.208	1.206	1.234	1.236	1.238	1.241	1.234
Overall	**7.436**	**7.199**	**7.684**	**7.634**	**7.582**	**7.481**	**7.333**

Stage	Stage Power (KW)						
	Case 1	Case 2	Case 3	Case 4	Case 5	Case 6	Case 7
1	892.4	833.0	634.5	617.1	725.8	811.6	865.3
2	892.4	864.6	725.5	725.8	885.1	897.5	918.2
3	892.4	889.8	1346.0	1562.8	1360.1	1155.1	1032.2
4	892.4	886.2	1435.8	1165.3	1038.3	1041.2	1011.4
5	892.4	888.3	942.3	962.5	975.3	995.2	961.6
6	892.4	889.9	966.7	973.7	979.3	991.7	974.3
7	892.4	886.1	934.7	939.9	944.8	953.0	949.2
8	892.4	885.8	923.2	925.9	929.0	934.6	935.1
Overall	**7139**	**7024**	**7909**	**7873**	**7838**	**7780**	**7647**

Stage	Rotor Work Coefficient						
	Case 1	Case 2	Case 3	Case 4	Case 5	Case 6	Case 7
1	0.737	0.718	0.528	0.513	0.604	0.675	0.720
2	0.737	0.746	0.604	0.604	0.736	0.747	0.764
3	0.737	0.767	1.120	1.300	1.132	0.961	0.859
4	0.737	0.764	1.195	0.969	0.864	0.866	0.841
5	0.737	0.766	0.784	0.801	0.811	0.828	0.800
6	0.737	0.767	0.804	0.810	0.815	0.825	0.811
7	0.737	0.764	0.778	0.782	0.786	0.793	0.790
8	0.737	0.764	0.768	0.770	0.773	0.778	0.778

Stage	de Haller Number						
	Case 1	Case 2	Case 3	Case 4	Case 5	Case 6	Case 7
1	0.726	0.737	0.846	0.855	0.803	0.762	0.736
2	0.726	0.727	0.851	0.854	0.773	0.755	0.736
3	0.726	0.716	0.666	0.592	0.615	0.668	0.696
4	0.726	0.716	0.586	0.652	0.688	0.691	0.695
5	0.726	0.715	0.709	0.705	0.702	0.700	0.707
6	0.726	0.713	0.694	0.693	0.693	0.692	0.698
7	0.726	0.715	0.699	0.699	0.699	0.698	0.701
8	0.726	0.715	0.699	0.699	0.699	0.699	0.702

Table A3 Non-equilibrium data (Droplet temperature, diameter, evaporation/boiling time, residence time) for all cases

Stage	Droplet Temp. (K)			
	Case 4	Case 5	Case 6	Case 7
1	288.0	288.0	288.0	288.0
1.5	289.9	289.5	289.2	288.7
2	292.7	291.8	291.1	289.8
2.5	294.5	293.8	292.7	290.8
3	297.7	297.3	295.9	292.9
3.5	304.1	302.2	299.6	295.0
4	351.0	319.0	308.6	299.0
4.5	392.4	389.7	318.4	302.6
5	398.3	395.5	339.5	308.8
5.5	428.6	426.5	369.3	314.1
6	433.9	431.8	428.2	322.5
6.5	463.9	462.2	459.4	329.6
7	469.5	467.8	464.9	340.8
7.5	497.7	496.2	493.8	350.2
8	503.5	501.9	499.4	364.7
8.5	530.5	529.2	527.1	376.6

Stage	Droplet Dia(μm)			
	Case 4	Case 5	Case 6	Case 7
1	9.573	14.359	19.145	28.718
1.5	8.666	13.475	18.491	28.295
2	8.647	12.482	16.105	23.684
2.5	6.828	10.727	14.641	22.598
3	6.828	8.841	12.569	21.243
3.5	4.790	7.139	11.200	20.321
4	0.000	3.415	8.986	19.101
4.5		0.000	7.345	18.264
5			4.349	17.135
5.5			0.678	16.352
6			0.000	15.288
6.5				14.551
7				13.534
7.5				12.828
8				11.854
8.5				11.198

Stage	Evap./ Boil. Time (ms)			
	Case 4	Case 5	Case 6	Case 7
1	0.3900	0.8775	1.5600	3.5852
1.5	0.1753	0.3765	0.6440	1.4101
2	0.1475	0.2798	0.4349	0.8602
2.5	0.1112	0.2423	0.4107	0.9277
3	0.0940	0.1497	0.2712	0.6985
3.5	0.0559	0.1116	0.2441	0.7715
4	0.0000	0.0278	0.1457	0.5778
4.5		0.0000	0.1142	0.6375
5			0.0426	0.4739
5.5			0.0019	0.5207
6			0.0000	0.3837
6.5				0.4208
7				0.3106
7.5				0.3411
8				0.2580
8.5				0.2910

Stage	Residence Time (ms)			
	Case 4	Case 5	Case 6	Case 7
1	0.1048	0.1048	0.1048	0.1048
1.5	0.1460	0.1493	0.1511	0.1519
2	0.0705	0.0731	0.0755	0.0771
2.5	0.1027	0.1080	0.1080	0.1080
3	0.0478	0.0521	0.0559	0.0593
3.5	0.0897	0.0860	0.0870	0.0898
4	0.0467	0.0488	0.0484	0.0495
4.5	0.0747	0.0740	0.0742	0.0764
5	0.0426	0.0422	0.0415	0.0423
5.5	0.0656	0.0652	0.0644	0.0656
6	0.0365	0.0363	0.0359	0.0361
6.5	0.0573	0.0570	0.0566	0.0568
7	0.0321	0.0319	0.0316	0.0316
7.5	0.0504	0.0502	0.0499	0.0498
8	0.0282	0.0281	0.0279	0.0278
8.5	0.0445	0.0444	0.0442	0.0440

Table A4 Liquid and phase data for fogging cases

Stage	Liquid Water Fraction				
	Case 3	Case 4	Case 5	Case 6	Case 7
1	0.01754	0.01754	0.01754	0.01754	0.01754
1.5	0.01282	0.01301	0.01450	0.01581	0.01678
2	0.01264	0.01293	0.01152	0.01044	0.00984
2.5	0.00610	0.00637	0.00731	0.00785	0.00855
3	0.00610	0.00637	0.00410	0.00496	0.00710
3.5	0	0.00220	0.00216	0.00351	0.00622
4	0	0	0.00024	0.00181	0.00516
4.5	0	0	0	0.00099	0.00451
5	0	0	0	0.00021	0.00373
5.5	0	0	0	0	0.00324
6	0	0	0	0	0.00265
6.5	0	0	0	0	0.00228
7	0	0	0	0	0.00184
7.5	0	0	0	0	0.00156
8	0	0	0	0	0.00123
8.5	0	0	0	0	0.00104

Stage	Water Vapor Fraction				
	Case 3	Case 4	Case 5	Case 6	Case 7
1	0.01596	0.01596	0.01596	0.01596	0.01596
1.5	0.02069	0.02049	0.01901	0.01770	0.01673
2	0.02087	0.02058	0.02199	0.02307	0.02367
2.5	0.02741	0.02714	0.02619	0.02566	0.02496
3	0.02741	0.02714	0.02941	0.02854	0.02641
3.5	0.03351	0.03131	0.03135	0.03000	0.02729
4	0.03351	0.03351	0.03327	0.03170	0.02835
4.5	0.03351	0.03351	0.03351	0.03252	0.02900
5	0.03351	0.03351	0.03351	0.03330	0.02978
5.5	0.03351	0.03351	0.03351	0.03351	0.03027
6	0.03351	0.03351	0.03351	0.03351	0.03086
6.5	0.03351	0.03351	0.03351	0.03351	0.03123
7	0.03351	0.03351	0.03351	0.03351	0.03167
7.5	0.03351	0.03351	0.03351	0.03351	0.03195
8	0.03351	0.03351	0.03351	0.03351	0.03227
8.5	0.03351	0.03351	0.03351	0.03351	0.03247

Table A5 Rotor-stator camber line geometries and stage information. Incidence angle i is for the i-th rotor stage and deviation angle δ is for the flow leaving i+0.5th stator.

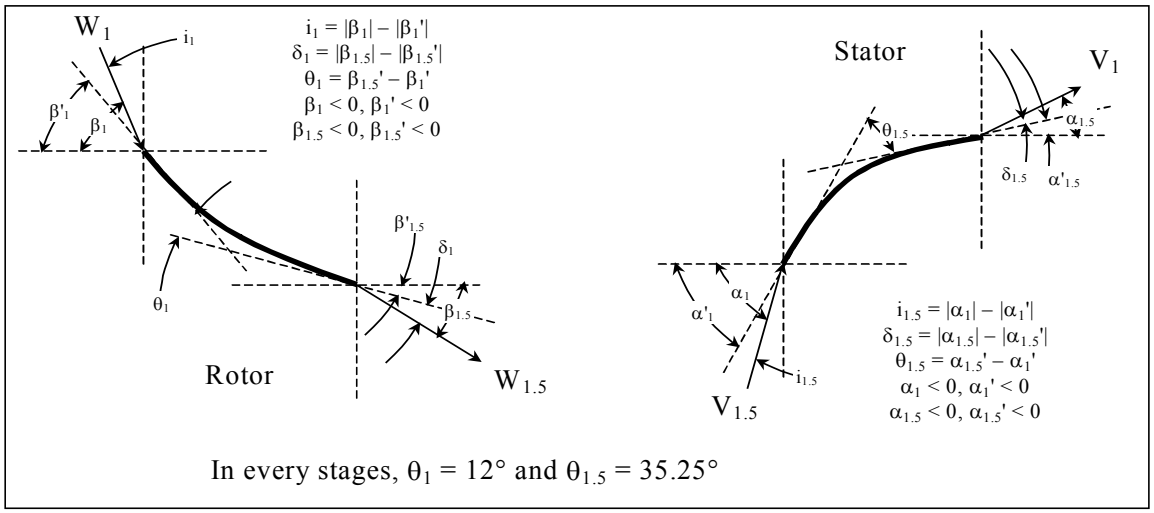

Stage	Hub to Tip Ratio	Tip Dia. (m)	Hub Dia. (m)	Chord Length (cm)	ß1' / ß1.5'	α1' / α1.5'	Case 1		Case 2		Case 3		Case 4		Case 5		Case 6		Case 7	
							i1 / δ1	i1.5 / δ1.5	i1 / δ1	i1.5 / δ1.5	i1 / δ1	i1.5 / δ1.5	i1 / δ1	i1.5 / δ1.5	i1 / δ1	i1.5 / δ1.5	i1 / δ1	i1.5 / δ1.5	i1 / δ1	i1.5 / δ1.5
1	0.636	0.560	0.356	3.400	-62.47	0.00	0.00	0.00	0.00	0.00	0.00	0.00	0.00	0.00	0.00	0.00	0.00	0.00	0.00	0.00
1.5	0.691	0.542	0.374	2.794	-50.47	35.25	0.00	0.00	0.00	-1.07	0.00	-11.76	0.00	-12.54	0.00	-7.59	0.00	-3.55	0.00	-0.97
2	0.703	0.538	0.378	2.658	-62.47	0.00	0.00	0.00	0.39	-1.07	1.89	-11.76	1.94	-12.54	3.22	-7.59	4.26	-3.55	4.98	-0.97
2.5	0.744	0.525	0.391	2.240	-50.47	35.25	0.00	0.00	0.39	-1.01	1.89	-22.01	1.94	-22.91	3.22	-12.14	4.26	-7.68	4.98	-4.28
3	0.757	0.521	0.395	2.111	-62.47	0.00	0.00	0.00	0.93	-1.01	3.76	-22.01	3.83	-22.91	6.54	-12.14	5.82	-7.68	4.47	-4.28
3.5	0.786	0.513	0.403	1.833	-50.47	35.25	0.00	0.00	0.93	-0.24	3.76	-14.31	3.83	-6.74	6.54	-2.55	5.82	-3.63	4.47	-2.80
4	0.797	0.510	0.406	1.721	-62.47	0.00	0.00	0.00	1.28	-0.24	4.79	-14.31	4.92	-6.74	5.34	-2.54	5.05	-3.63	3.84	-2.80
4.5	0.818	0.504	0.412	1.529	-50.47	35.25	0.00	0.00	1.28	0.10	4.79	0.40	4.92	-0.60	5.34	-1.17	5.05	-2.17	3.84	-1.15
5	0.828	0.501	0.415	1.434	-62.47	0.00	0.00	0.00	1.51	0.10	2.94	0.40	3.19	-0.60	3.49	-1.17	3.92	-2.17	3.16	-1.15
5.5	0.844	0.497	0.419	1.292	-50.47	35.25	0.00	0.00	1.51	0.34	2.94	0.37	3.19	-0.08	3.49	-0.47	3.92	-1.20	3.16	-0.75
6	0.853	0.494	0.422	1.212	-62.47	0.00	0.00	0.00	1.64	0.34	2.22	0.37	2.41	-0.08	2.61	-0.46	2.94	-1.20	2.75	-0.75
6.5	0.865	0.491	0.425	1.106	-50.47	35.25	0.00	0.00	1.64	0.58	2.22	2.18	2.41	1.81	2.61	1.44	2.94	0.83	2.75	0.73
7	0.873	0.489	0.427	1.039	-62.47	0.00	0.00	0.00	1.69	0.58	1.60	2.18	1.74	1.81	1.88	1.44	2.11	0.83	2.21	0.73
7.5	0.882	0.487	0.429	0.957	-50.47	35.25	0.00	0.00	1.69	0.61	1.60	3.21	1.74	2.94	1.88	2.64	2.11	2.14	2.21	1.75
8	0.889	0.485	0.431	0.901	-62.47	0.00	0.00	0.00	1.70	0.61	1.13	3.22	1.25	2.94	1.37	2.64	1.56	2.14	1.77	1.76
8.5	0.896	0.483	0.433	0.836	-50.47	35.25	0.00	0.00	1.70	0.60	1.13	4.16	1.25	3.90	1.37	3.63	1.56	3.20	1.77	2.61